

THE EFFECT OF PRECIPITATE DISTRIBUTION ON FATIGUE CRACK PROPAGATION IN  
A POWDER-FORMED SUPERALLOY (AP1)

S.A. MORLEY and J.W. MARTIN\*

Fatigue crack propagation tests were conducted at room temperature and at 600°C on CCT specimens of AP1 with average  $\gamma'$  particle size varying between 0.13 $\mu\text{m}$  and 0.05 $\mu\text{m}$ , as well as with a duplex  $\gamma'$  distribution.

At intermediate  $\Delta K$  levels, at room temperature, fatigue crack growth rates were lowest in the microstructure containing a single distribution of fine  $\gamma'$  precipitates. At 600°C the opposite effect was observed, in that the microstructure containing the coarsest  $\gamma'$  showed the best resistance to fatigue crack propagation.

The room temperature results are interpreted in terms of the effect of  $\gamma'$  on slip distribution. At 600°C the crack is observed to be mainly confined to the  $\gamma$  matrix.

1. INTRODUCTION

Nimonic AP1 is a powder-formed nickel-based superalloy which has a potential application as a disc material in aero gas turbines. An understanding of the factors influencing fatigue crack propagation, particularly at elevated temperatures, is important in the prediction of safe component lives.

In the near-threshold regime, it has been shown by King (1) that the fatigue crack propagation characteristics at room temperature of this material are highly microstructurally sensitive, in particular with regard to the grain size and the  $\gamma'$ -distribution. Sadananda and Shahinian (2) have reviewed in detail the subject of crack growth at high temperatures, and point out that it is advantageous to characterise crack growth in the creep range on the basis of the micromechanics of the growth processes. In their study of single crystals of MAR MOO2, Crompton and Martin (3) have found that, at low and intermediate levels of  $\Delta K$ , the elevated temperature crack growth behaviour is not attributable to environmental interactions but is influenced by the morphology and distribution of the strengthening  $\gamma'$  precipitate.

The development of complex, HIP'ed superalloys has enabled specimens with a controlled range of microstructures to be produced, and the present work describes an investigation of the effect of differing  $\gamma'$  particle distributions on fatigue crack propagation at room temperature and at 600°C. The effect of  $\gamma'$  in fatigue has been correlated with observations of the crack tip deformation characteristics of the alloy employing scanning electron microscopy.

\* (Oxford University, Department of Metallurgy & Science of Materials, UK)

## 2. EXPERIMENTAL MATERIALS AND METHODS

The material was produced from hot isostatically pressed ('HIP'ed) powder, and the composition of the alloy is given in Table 1.

Table 1: Composition of alloy Nimonic AP1 (wt%)

Al 4.0;	Ti 3.4;	Mo 5.2;	Cr 15.4;
Co 17.0;	B 0.024;	C 0.03;	Ni balance

The alloy was solution-treated at 1150°C for 2 hr followed by air-cooling. Ageing treatments between 650°C and 800°C for 24 hr were applied in order to produce varying dispersions of the  $\gamma'$  phase.

C.C.T. specimens were prepared in accordance with A.S.T.M. E647-78T by spark machining to the appropriate dimensions (30mm x 2mm x 105mm). Fatigue tests were conducted in air at room temperature and at 600°C, using a servo-hydraulic testing machine operating under conditions of constant  $\Delta K$  at an R value of 0.1. Triangular loading at a test frequency of 10 Hz was applied. Crack extension was monitored using a DC potential drop method which enabled absolute values of crack length to be determined to within 0.05mm.

## 3. EXPERIMENTAL RESULTS

### 3.1 Microstructures

Fig. 1 is an optical micrograph showing the structure typical of all the alloys. Grain boundaries and prior particle boundaries (P.P.B.s) are both clearly defined. At high magnification the grain boundaries were seen to be highly serrated. The grain size measured by a mean linear intercept method was between 40  $\mu\text{m}$  and 45  $\mu\text{m}$ , and the PPB size was typically 130  $\mu\text{m}$ .

The  $\gamma'$  precipitate sizes were determined by transmission electron microscopy using superlattice reflections (Fig. 2), where they are seen to possess a rounded cuboidal morphology. Three distributions of  $\gamma'$  particles have been studied, and these are defined in Table 2:

Table 2

Alloy	Mean $\gamma'$ particle size ( $\mu\text{m}$ )
C2	0.13
C1	0.08
F	0.05
D (duplex)	0.12 + (0.03-0.05)

### 3.2 Fatigue Crack Growth Rates

The results for the fatigue crack propagation tests at room temperature and at 600°C are shown in Figs. 3 and 4 respectively.

At room temperature (Fig. 3), microstructures F and D gave similar growth rates over the range of  $\Delta K$  applied, while microstructure C1 gave slightly higher growth rates.

At 600°C (Fig. 4) it is seen that the opposite effect is found. Microstructures F and D again gave similar growth rates over the range tested, but

microstructures C1 and C2 show progressively slower crack propagation rates at a given applied  $\Delta K$ . Comparison of Figs. 3 and 4 reveals that both D and F gave faster growth rates at 600°C than at room temperature, microstructure C1 showed little or no change in growth rates with increase in temperature.

### 3.3 Fractography

At room temperature, all the microstructures showed predominantly crystallographic crack growth at growth rates up to about  $10^{-4}$  mm/cycle. A typical fracture surface is shown in Fig. 5, where large relatively smooth areas can be seen within individual grains, and straight slip-type markings can be seen on many of these facets. Crystallographic steps can also be observed within grains, and some small areas between facets show round holes, where failure has occurred around grain boundaries or PPBs.

At high growth rates, all microstructures again exhibited similar features (Fig. 6). Large rounded features with dimpled surfaces can be clearly seen; their size ranges from 50  $\mu\text{m}$  to 130  $\mu\text{m}$  and they represent failure along prior particle boundaries.

Crack growth at high temperature also appeared to be crystallographic, and was similar for all microstructures. Areas of crystallographic slip appeared, however, to be more ragged than those formed at room temperature. Under conditions of high  $\Delta K$ , failure, as at room temperature, was observed round PPB particles and around grain boundaries.

## 4. DISCUSSION

### 4.1 High growth rate behaviour

Failure along the PPBs (Fig. 6) has been reported by Bressers et al (4) in PM Astroloy in low strain amplitude low cycle fatigue tests at 730°C in vacuum. In the present tests it appears that the frequency and crack growth rate are too high for oxygen diffusion to cause embrittlement of the grain boundaries, and failure along the PPBs occurs in preference to intergranular cracking. The prior particle boundaries are decorated with discrete spherical carbides typically 1-2  $\mu\text{m}$  in diameter, separated by distances of the same order. Under these conditions of high  $\Delta K$ , the size of the crack-tip plastic zone is comparable with the spacing of the PPBs, and this can give rise to decohesion of the particle-matrix interface or to cracking of the carbides ahead of the crack tip. Crack advance will occur by the ductile rupture of the intervening ligaments, causing the crack to follow the PPB, leaving a round, dimpled feature on the fracture surface (Fig. 6).

### 4.2 Intermediate growth rates

4.2.1 Room temperature behaviour. The observations of room temperature behaviour are broadly in accordance with those of King (1). At lower values of  $\Delta K$ , the size of the crack tip reverse plastic zone will be less than the spacing of the PPBs or the grain boundaries. Deformation processes within the grains will therefore lead to the observed crystallographic crack growth. In AP1 and other nickel alloys strengthened by the presence of coherent  $\text{Ni}_3$  (Ti, Al) ( $\gamma'$ ) precipitates, intense slip bands form during both monotonic and fatigue deformation due to the shearing of the ordered precipitates by the glide dislocations. This accounts for the observation of crack growth on  $\{111\}$  planes at room temperature.

At room temperature, microstructure C1 showed faster growth rates than microstructures F and D (which showed similar growth rates). This similarity

of behaviour of the duplex  $\gamma'$  and the fine  $\gamma'$  specimens suggests that the crack growth behaviour in D is controlled by the fine  $\gamma'$  phase (which is the same in both microstructures). Examination of an etched, interrupted fatigue crack propagation specimen of D (Fig. 7) shows that the crack rarely cuts the coarse  $\gamma'$  precipitates in D so the crack is confined to the regions containing the fine  $\gamma'$  particles.

Comparing now structures F and C1, the coarser  $\gamma'$  precipitates in C1 will be more widely separated than those in F. This implies that glide dislocations will, on average have a larger glide distance in the  $\gamma$  matrix of C1 than in F. The possibility of cross-slip will therefore be greater in C1 than in F, so that microstructure C1 would thus be expected to exhibit a more homogeneous slip distribution than microstructure F. Hornbogen and Zum Gahr (5) have proposed that microstructures tending towards heterogeneous slip should show lower fatigue crack propagation rates, because the concentration into intense bands can allow partial reversal of primary slip activity in any cycle and thus a reduction in the amount of crack advance for that cycle.

**4.2.2 Fatigue at 600°C.** At 600°C microstructures F and D again showed similar growth rates over the range tested, but these rates were faster than those obtained in microstructures C1 and C2. It is proposed that the differences in growth rates at 600°C in the different microstructures are due to the operation of a mechanism for crack advance that involves bypass of the  $\gamma'$  precipitates.

The yield stress of the  $\gamma'$  phase is known to increase with rising temperature to reach a peak at 700°C (Davies and Stoloff, (6)). In contrast, the flow stress of the  $\gamma$  matrix will fall with increasing temperature, as dislocation climb around obstacles in the slip plane becomes easier. Crompton and Martin (3) have found that this effect leads to a change in fatigue crack growth mechanism at high temperatures in single crystal MAR MOO2. They found that, at elevated temperatures, fatigue crack growth took place predominantly on the  $\gamma$  matrix; the cuboidal  $\gamma'$  particles in the alloy were aligned over long distances with their faces parallel to {100}, and crack growth was thus constrained to give macroscopic failure on {100}.

In the present material the  $\gamma'$  particles are not aligned along  $\langle 100 \rangle$  over distances which are large compared to the interparticle spacing. A crack in the  $\gamma$  matrix must therefore follow a more convoluted path compared (for example) to a matrix crack in single crystal MAR MOO2 (ref. 3). The degree of convolution will increase with increasing size of the  $\gamma'$  particles, and this can account for the decrease in  $da/dN$  as the average particle size of the  $\gamma'$  is increased on passing from F to C1 to C2. Examination of etched, interrupted fatigue test propagation specimens of microstructure C1 tested at 600°C imaged in the SEM showed that the crack does indeed tend to bypass the  $\gamma'$  precipitates, and only occasionally cuts through them.

## 5. CONCLUSIONS

1. In the microstructure containing a duplex distribution of  $\gamma'$  precipitates, the fine  $\gamma'$  particles appear to control the fatigue crack growth behaviour.
2. Crack growth rates at room temperature were slower in the microstructures containing fine  $\gamma'$  precipitates due to the greater slip reversibility in this microstructure.
3. At 600°C, fatigue crack growth occurred in the  $\gamma$  matrix, and  $\gamma'$  precipitates were rarely cut by the crack. This resulted in lower crack prop-

agation rates in the microstructure containing a coarse  $\gamma'$  precipitate distribution, since this involves a more convoluted fracture path.

## ACKNOWLEDGEMENTS

The authors are grateful to Professor Sir Peter Hirsch, FRS, for the laboratory facilities made available, to the Procurement Executive of the Ministry of Defence for support, and to Dr J S Crompton for valuable discussions.

## SYMBOLS USED

$\Delta K$	=	stress intensity range (MPa $m^{1/2}$ )
$K_{max}$	=	maximum stress intensity factor (MPa $m^{1/2}$ )
$K_{min}$	=	minimum stress intensity factor (MPa $m^{1/2}$ )
R	=	$K_{min}/K_{max}$
$da/dN$	=	crack growth rate per cycle (nm/cycle)

## REFERENCES

1. King, J.E., Metal Science, **16**, (1982) 345.
2. Sadananda, K. and Shahinian, P., "Cavities and Cracks in Creep and Fatigue", (Appl. Science Publishers, London, England, 1981), 109.
3. Crompton, J.S. and Martin, J.W., Met Trans. (A), (1984) in the press.
4. Bressers, J., Roth, M., Fenske, E., and Tambuyser, P., "High Temperature Alloys for Gas Turbines 1982", ed. R. Brunetaud, D. Coutsouradis, T.B. Gibbons, D.B. Meadowcroft, R. Stickler, (D. Reidel Publ. Co., Dordrecht, Holland, 1982), 597.
5. Hornbogen, E., and Zum-Gahr, K.H., Acta Met., **24**, (1976), 581.
6. Davies, R.G. and Stoloff, N.S., Trans. AIME, **233**, (1965), 714.

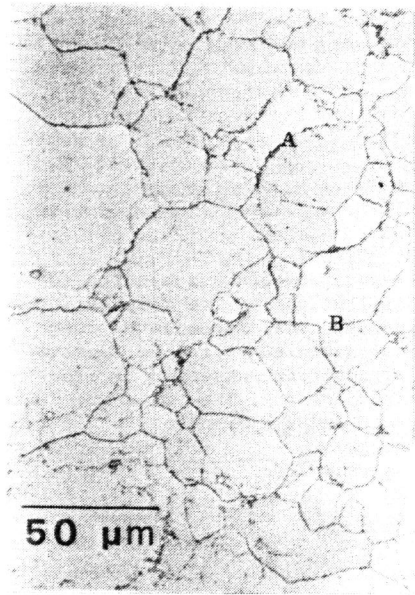


Fig. 1 Optical micrograph of Alloy T showing prior particle boundaries (A) and grain boundaries (B).

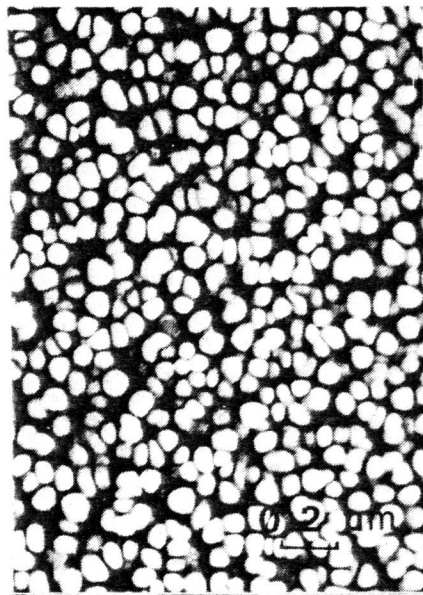


Fig. 2 Dark field TEM micrograph of microstructure F.

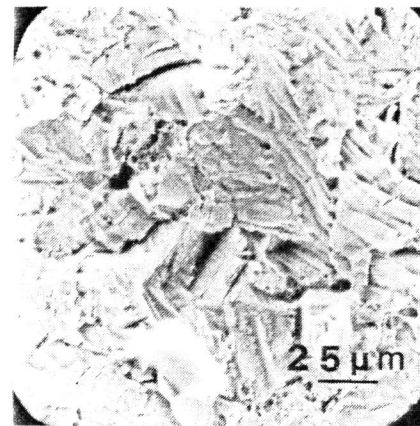


Fig. 5 Room temperature fracture surface of microstructure F.

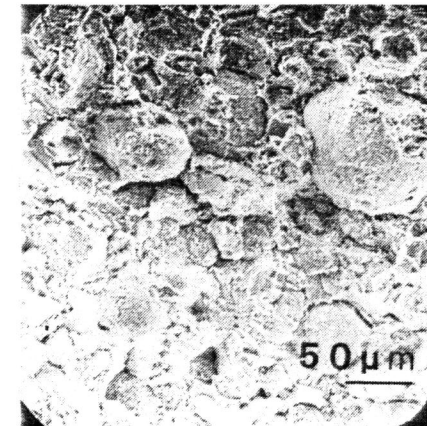


Fig. 6 Fracture surface for microstructure C1: high  $da/dN$  at room temperature.

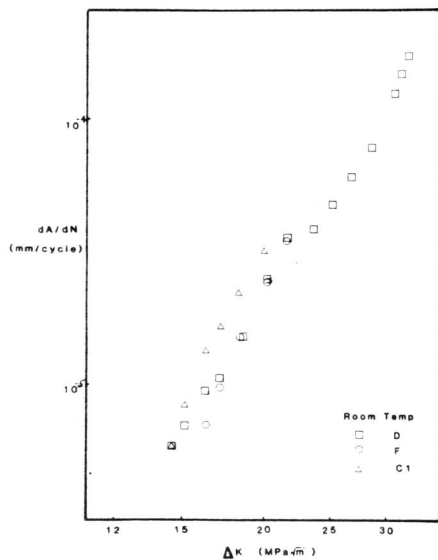


Fig. 3 Fatigue crack growth rate curves for microstructures C1, F and D at room temperature.

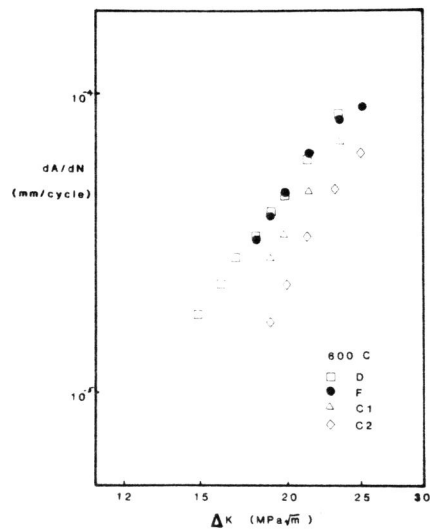


Fig. 4 Fatigue crack growth rate curves for microstructures C1, C2, F & D at 600°C.

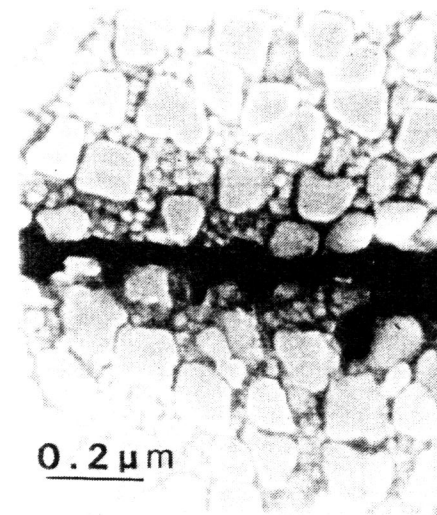


Fig. 7. SEM micrograph of fatigue crack at room temperature in microstructure D, showing the crack mainly bypassing the coarse  $\gamma'$  precipitates.